N_2 emission-channel change in NO reduction over stepped Pd(211) by angle-resolved desorption

Tatsuo Matsushima,[a,e*] Anton Kokalj,[b] Hideo Orita,[c] Toshitaka Kubo,[d] Masataka Sakurai,[e] Takahiro Kondo,[e] and Junji Nakamura[e]

[a] Catalysis Research Center, Hokkaido University, Sapporo, 001-0021, Japan

[b] Jozef Stefan Institute, Jamova 39, 1000 Ljubljana, Slovenia

[c] Nanosystem Research Institute (NRI), National Institute of Advanced Industrial Science and Technology (AIST), Tsukuba Central 2, 1-1-1 Umezono, Tsukuba, Ibaraki 305-8568, Japan

[d] Nanosystem Research Institute (NRI), National Institute of Advanced Industrial Science and Technology (AIST), Tsukuba Central 5, 1-1-1 Higashi, Tsukuba, Ibaraki 305-8565, Japan

[e] Faculty of Pure and Applied Sciences, University of Tsukuba, Tennodai 1-1-1,Tsukuba, Ibaraki 305-8573, Japan

* Corresponding author; Tatsuo Matsushima

Tel/Fax; +81-29-874-1508

E-mail; tatmatsu@mbr.nifty.com

Postal address; Catalysis Research Center, Hokkaido University, Sapporo, 001-0021, Japan

Abstract

A sharp change in the N_2 emission channel from $N_2O(a) \rightarrow N_2(g)+O(a)$ to $N(a)+N(a) \rightarrow N_2(g)$ has been found at around 500 K in a steady-state $NO+D_2$ reaction over stepped Pd(211)= [(S)3(111)×(100)] by means of angle-resolved desorption. The desorbing N_2 is highly collimated at around 30° off normal toward the step-down direction below about 500 K due to the intermediate N_2O decomposition, whereas, above 500 K, the near normally directed desorption due to the recombination of N(a) is relatively enhanced. The N_2O decomposition channel is promoted when the reaction is carried out with hydrogen (deuterium) and the channel change is accelerated by quick changes of the amounts of surface hydrogen and oxygen (or NO(a)) into the opposite directions, and enhanced nitrogen removal as ammonia on the resultant hydrogen-rich surface. In the steady-state NO+CO reaction, the N_2 emission channel gradually changes above 500 K toward recombination. A model for the off-normal N_2 emission is briefly described.

Key words; Nitrogen oxide, Nitrous oxide, Reduction, Nitrogen, Palladium, Stepped surface

1. Introduction

The N_2 emission in the steady-state NO reduction on palladium and rhodium, the best deNOx catalysts, takes place through either (i) an $N_2O(a)$ intermediate, which then decomposes to $N_2(g)+O(a)$, or (ii) $N(a)+N(a)\rightarrow N_2(g)$ [1]. This paper reports a sharp change in the N_2 emission channel at around 500 K from $N_2O(a)\rightarrow N_2(g)+O(a)$ toward the $N(a)+N(a)\rightarrow N_2(g)$ reaction in the steady-state $NO+D_2$ reaction on stepped Pd(211)=[(S)3(111)×(100)] and the limited extent of the channel change in the NO+CO reaction over the range of 450 K to 700 K. The N_2O decomposition channel is promoted when the reaction is carried out with hydrogen (deuterium) and then the channel change is accelerated by quick changes of surface oxygen (or NO(a)) and hydrogen into the opposite directions, and enhanced N(a) removal as ammonia on the resultant hydrogen-rich surface. The two different N_2 emission channels mentioned above can be separately examined by angle-resolved (AR) desorption because, in the N_2O decomposition channel, the product N_2 is sharply emitted off normal, whereas, in the nitrogen recombination, it is desorbed nearly along the surface normal in a broader form.

The above off-normal N_2 emission was first found in temperature-programmed desorption (TPD) of NO-covered Pd(110) by Ikai and Tanaka [2-4]. Using an isotope tracer, they confirmed that, on Pd(110) and stepped Pd(211), this N_2 comes from the reaction of NO(a) with N(a); i.e., the heating of a surface with $^{15}N(a)$ and $^{14}NO(a)$ results in the emission of $^{14}N^{15}N$ off normal and $^{15}N_2$ along the surface normal [5,6]. For the peculiar N_2 emission, they proposed a desorption-mediated reaction model in which desorbing NO was suggested to affect this off-normal emission. Although a significant amount of product N_2O was found in the temperature range of the off-normal N_2 emission in their TPD work as well, they omitted the decomposition (before desorption) of intermediate $N_2O(a)$ toward N_2 [5,6]. Furthermore, from the absence of such inclined N_2 emission in the subsequent cooling in the presence of H_2 and NO, they argued that this off-normal desorption channel is not involved in the catalyzed NO reduction [7,8]. On the other hand, Matsushima *et al.* reproduced this inclined N_2 emission *in the absence of NO(a)* in TPD procedures of N_2O-covered Pd(110), Rh(110), Ir(110), and Rh(100) or N_2O exposures on clean Rh(110) above 60 K, as well as the steady-state NO or N_2O reduction on Pd(110), Rh(110), and Rh(100) [1,9]. The lack of difference in the desorption dynamics (spatial and/or velocity distributions) of hyper-thermal product N_2 between steady-state NO+CO (or H_2) below about 550 K and thermal decomposition or reduction of N_2O indicates the off-normal product emission from *a common transition state* [1] and moreover that the state of desorbing NO has no effects on the off-normal emission.

These findings have, at long last, confirmed the participation of intermediate N_2O in the main pathway of catalyzed NO reduction to N_2 on Pd and Rh. In fact, this intermediate or N_2O-like transition state emitting N_2 has been frequently proposed in kinetic simulations [10-14]. The origin of the inclined N_2 emission is due to the decomposition of N_2O oriented along the [001] direction.

The oriented N_2O was later confirmed on Pd(110) by scanning tunneling microscopy [15] and near-edge X-ray absorption fine structure [16] as well as density functional theory (DFT) with generalized gradient approximation (GGA) on Pd(110) and Rh(110) [17,18]. According to the last AR measurements providing three-dimensional (3D) distributions, the inclined N_2 emission is highly concentrated around the normally directed plane along the [001] direction on Pd(110) and Rh(110) [19-21]; i.e., the orientation of the parent N_2O is preserved in the spatial distribution of desorbing N_2 even at high temperatures around 800 K.

The pathway to N_2 via the intermediate N_2O has the potential to remove nitrogen on catalyst surfaces even at around room temperature because of its fast formation and decomposition [1,22,23]. It may play a major role in surface nitrogen removal, for example, in automobile gas convertors (involving active Pt-Rh sites [7,24]) working at the start of a cold engine or in the catalyzed reduction of aqueous nitrate and nitrite ions [25-27]. However, its kinetic and dynamic behavior is still unclear. Only AR-desorption analysis can selectively examine this process because of the absence of spectroscopic observations of N_2O(a) in the course of catalyzed deNOx processes [28,29]. Stepped Pd(211) provides a stage suitable to examine this pathway because it is rather stable toward reconstructions [30] and significantly produces N_2O in the NO reduction as observed on other stepped Pd surfaces [31,32].

2. Experimental

The apparatus consists of three ultrahigh-vacuum chambers as described previously [33]. Briefly, a reaction chamber has low-energy electron diffraction (LEED), X-ray photoelectron spectroscopy optics, and a mass spectrometer for angle-integrated (AI) signals in an analog mode. An analyzer, which is separately evacuated, has a mass spectrometer for angle-resolved (AR) measurements with a pulse counting mode. The chopper house between the reaction chamber and the analyzer is rapidly and separately evacuated. The N_2 flux is measured with the AR mass spectrometer without sensitivity corrections due to different velocities as a function of the desorption angle (θ; polar angle) because no serious shift is caused when constructing the angular distribution [20]. The angle is scanned in the normally directed plane along the [$\bar{1}$11] (step up-and-down) direction (see Fig. 1) because of the maximized product N_2 desorption in the decomposition of adsorbed N_2O on Pd(211) [34]. The polar angle sign is defined as negative on the side of inclined N_2 emission, referring to Ikai-Tanaka's work (Fig. 1) [5].

A palladium crystal (from *Surface Preparation Laboratory*, Netherlands) in a disk-shape slice was mounted on the top of a manipulator. The LEED pattern showed a sharp (1×1) form after cleaning by Ar^+ ion bombardments, heating in oxygen, and subsequently reducing in D_2. Without further purification, commercial ^{15}NO (isotope purity: 99%), D_2 (purity: 99%) and ^{13}CO (purity: 99%) were separately backfilled. Hereafter, isotopes ^{15}N and ^{13}C are simply designated as N and C in the text.

The AI- or AR signal is determined as the signal difference between a desired surface temperature and room temperature.

3. Results

3.1 Temperature dependence

The steady-state NO+D_2 reaction is noticeable above T_S (surface temperature)=410 K and shows a steep N_2 peak at around 475 K and a broad one above 550 K (Fig. 2(a)). The AR-N_2 signal is monitored at θ=-31° off normal, which is the collimation (maximum flux) angle. It is well reproduced in the subsequent cooling. The former peak is large in the AR form but small in the AI form. The ratio of the AR signal to the AI one is largely decreased above 500 K, indicating changes in the angular distribution. At high D_2 pressures (Fig. 2(b)), the N_2 formation peaks are well separated; i.e., the peak at 475 K is reduced, and the N_2 formation above 550 K is enhanced. In this case, the ammonia formation is significant, peaking at around 550 K. In general, at low D_2 pressures, the surface nitrogen deposited from NO dissociation is merely removed as N_2 since the amounts of formed N_2O and ND_3 are much lower (Fig. 2(a)). On the other hand, at high D_2 pressures, surface nitrogen is removed as N_2 and ND_3 depending on the surface temperature.

For comparison with the TPD work in Ikai-Tanaka's report [5], the AR-N_2 signal at θ =-31° was recorded while the surface was heated at a constant rate of 3.3 K/s in the presence of NO and D_2 as well as in the subsequent cooling (Fig. 3(a)). The sharp peak is observed at around 490 K only during heating, and the broad maximum around 600 K is reproduced in both procedures, as reported. The peak at 490 K becomes sharper at higher D_2 pressures and is suppressed at low pressures.

3.2 Angular distribution

The AR-N_2 signal at 490 K during TPD is shown against the desorption angle θ after being normalized to the unit surface area (Fig. 3(b)). It shows a distribution form of $\cos^{25}(\theta+30)$. On the other hand, the signal at 600 K shows a $\cos^2(\theta+5)$ form (Fig. 3(c)). By using the power series of the cosine of the desorption angle shift from the collimation angle, the observed distribution is de-convoluted into two components, a sharp component collimated around -30° as $\cos^{28}(\theta+30)$ and a broad one directed close to the surface normal. The factor R in the figure indicates the ratio of the maximum signal between the broad and sharp component. These distributions agree well with the results in the report by Ikai and Tanaka except for the very weak $\cos^2(\theta+5)$ component in the desorption at 490 K [5]. This may be due to the slower heating rate in the present work.

The AR-N_2 signal in the steady-state NO reduction is plotted versus the desorption angle in Fig. 4. The distribution is sensitive to the surface temperature, especially around 500 K. The N_2 desorption is sharply collimated around -30° off normal below about 490 K. Above 500 K, the signal in the normal direction is relatively increased, and the component collimated off normal is reduced.

At 590 K, the desorption flux is approximated as $\cos^{1.5}(\theta+5)$. The observed distribution is again de-convoluted into two power components of the cosine of the desorption angle shift, a sharp off-normal component and a broad one directed close to the surface normal. The factor *R* sharply increases around 500 K. Below 480 K, N_2 is mostly emitted into the inclined way, whereas, above 500 K, it mostly consists of the broad component. These results agree well with those in the TPD procedures. The resultant two desorption components are the main players to emit the product N_2 even in the steady-state NO reduction on stepped Pd as well [1]. The former inclined desorption is due to the decomposition of intermediate N_2O, and the latter comes from the recombination of adsorbed nitrogen atoms, as described in the Introduction [1]. The N_2 emission channel sharply changes from the decomposition of intermediate N_2O(a) to nitrogen atom recombination at around 500 K.

3.3 D_2 pressure effect

The N_2 emission channel change also depends on the hydrogen (deuterium) pressure. There is a critical deuterium pressure for N_2 emission. Below this point, the N_2 formation increases with increasing D_2 pressure but decreases or remains fairly constant above this point (Fig. 5). It should be noted that the ND_3 signal steeply increases above the critical point. The pathway of surface nitrogen removal changes toward ammonia formation, since the total NO consumption still increases with D_2 pressure, as seen from a continued increase of D_2O formation over the critical point and small amounts of N_2O formation. The ratio of the AR-N_2 signal at -31° to the AI-N_2 at 470 K somewhat decreases over the critical point, indicating a small contribution from the N(a) recombination; i.e., the decrease of N_2 signal is mostly due to the ammonia formation. At temperatures above 465 K, the ammonia formation is enhanced above the critical D_2 pressure. The kinetic transition point shifts to lower D_2 pressures at higher temperatures. The AI signals of D_2O and ND_3 are largely shifted to higher values in the procedure of decreasing D_2 pressure due to the memory of their adsorption on the chamber wall (Fig. 5).

The flash-desorption technique has been applied to determine the amounts of adsorbed species during the catalyzed NO reduction [35]. The crystal is heated from a steady-state condition at a fixed temperature to 930 K, where there are no adsorbed species except for oxygen, while AI signals due to D_2, D_2O, ND_3, N_2, NO, and N_2O are simultaneously monitored. The amount of surface nitrogen-containing species initially adsorbed (mostly NO(a) and N(a) [30,36]) is calculated as the sum of peak areas due to ND_3, N_2, NO, and N_2O although their amounts are not separately determined. Indeed, the peak areas of ND_3 and N_2O signals are negligible. With increasing P_{D2} at fixed $P_{NO}=1.5\times10^{-5}$ Pa and 460-480 K, the adsorbed N-containing species increases to the critical point and then decreases above it [35]. The amount of deuterium-containing species is negligible below the critical point, and above it, the amount is not determined because of the large memory effect of

D_2O signal.

3.4 NO+CO reaction

The temperature dependence of the steady-state NO+CO reaction is different from that for the NO+D_2 reaction; i.e., no sharp N_2 formation peak is found at around 480 K when CO is used (Fig. 6(a)). The reaction is noticeable above 410 K, increases sharply around 460 K, shows a broad maximum around 510 K, and then decreases at higher temperatures. In the subsequent cooling, both AI-N_2 and AI-CO_2 signals are well reproduced. The products from this reaction are N_2, CO_2 and a small amount of N_2O. The ratio of AI-signal CO_2 to that of N_2 is fortunately about 2 although these species may have differences in the mass spectrometer sensitivity and the pumping rate. The AR-N_2 signal at θ=-30° off normal (the collimation angle) also follows a similar temperature dependence except for the peak temperature around 490 K and faster decrease at higher temperatures. The AR/AI N_2 signal ratio is slowly decreased above 490 K, suggesting a slow change of the N_2 emission channel.

The AR-CO_2 signal normalized to the unit surface area at 531 K is plotted versus the desorption angle in Fig. 6(b). The desorption is collimated at around -10° off normal. By using a power series of the cosine of the desorption angle shift, the observed distribution is de-convoluted into two components, a sharp component collimated at -10° and a cosine one. The cosine component is always observed in desorbing CO_2 in the CO oxidation on palladium, showing a Maxwellian velocity distribution at the surface temperature [33]. The sharp component is approximated to a form of $\cos^{10}(\theta+13)$ at 450 K and $\cos^{14}(\theta+11.5)$ at 555 K. These distributions were well reproduced in the CO+O_2 reaction at a pressure ratio of P_{CO}/P_{O2}=2. It has been confirmed that the amount of surface CO in the steady-state NO+CO reaction is noticeable but below one fourth of the value equilibrium to the CO pressure (without NO), whereas the amount of surface N-containing species increases with increasing NO pressure.

The counter product N_2 desorption is sharply collimated at around -30° off normal over a wide temperature range (Figs. 6(c-d)). The distribution is again de-convoluted into two components, sharp off-normal and broader components, as shown by the broken curves. The inclined component is in a form of $\cos^{30}(\theta+30)$ at 475 K, $\cos^{20}(\theta+31)$ at 531 K, and $\cos^{12}(\theta+28)$ at 610 K (not shown for brevity). This component is major even at 531 K and relatively decreases with increasing surface temperature. The ratio R of the two components increases to 0.83 at 610 K.

4. Discussion

4.1 N_2 emission via intermediate N_2O

The N_2 emission channel from the decomposition of N_2O intermediate via the reaction of NO(a)+N(a) was not accepted on Pd and Rh surfaces until a long time after the earlier proposals as

described in the Introduction [10-12,14]. The emission of N_2O itself was treated as a bypath yielding a harmful byproduct [37]. For example, Belton *et al.* confirmed the fast N_2O formation from N(a)+NO(a) on Rh(111), but did not succeed in confirming the subsequent decomposition emitting N_2 [23,38]. The same N_2O(a) formation pathway was repeatedly proposed on open Pd surfaces such as Pd(110), stepped Pd(211) and Pd(331) or Pd(111) with defects since N_2O and N_2 as well are significantly found in TPD procedures of NO-covered surfaces at relatively low temperatures [30-32]. However, spectroscopic observations of N_2O(a) are not successful in the course of the catalyzed NO reduction on Pd and Rh surfaces with or without supporting materials [28,29,39]. This is in high contrast to the N_2O intermediate yielding N_2 on Cu-oxide or metal-exchanged zeolite catalysts, which has been supported with infrared spectroscopy [14]. The above consideration of N_2O species on Pd and Rh surfaces as un-reactive was merely due to the lack of direct evidence of N_2 emission from adsorbed N_2O before AR desorption analysis for steady-state NO reduction [1].

We consider the reason why adsorbed intermediate N_2O is not found with surface spectroscopy. The adsorption heat of N_2O on Pd(110), about 35 kJ mol^{-1}, is larger than the activation energy of N_2O(a) dissociation to N_2 and O(a) [1,40,41]. This tendency is common on open surfaces such as Pd(211) [34], Rh(110), Rh(100), Ir(110), and Ni(775) [42]; i.e., the intermediate N_2O(a) quickly decomposes and desorbs as well, yielding a very short life time at high temperatures for NO reduction although its branching to decomposition/desorption largely depends on the amount of co-adsorbed species and the surface temperature [1,41,43]. An estimated surface residence time of N_2O is on the order of nanoseconds, which is not long enough to allow detection of the species with surface vibration spectroscopy [29,30,39]. On the other hand, such a short surface residence is still long enough for nascent N_2O(a) on Pd and Rh surfaces to be oriented into a direction suitable for dissociative adsorption because of no differences in the desorption dynamics of desorbing N_2 between steady-state NO+CO (or H_2) below about 550 K and thermal decomposition or reduction of N_2O. It is also consistent with the fact that un-reacted N_2O is found in the products at low temperatures where the N_2O decomposition channel prevails. AR product desorption analysis for the NO or N_2O reduction on Pd(110), Rh(110) and Rh(100) shows the inclined N_2 emission characterizing the decomposition of oriented N_2O even at 700-800 K [1]. In fact, the collimation angle for this off-normal emission is insensitive to the surface temperature from 60 K to 800 K.

In general, the transition state (TS) of the process N(a)+NO(a)→N_2O(a) is different from that for the subsequent dissociation N_2O(a)→N_2(g)+O(a). The first TS is horse-like, where (N-N-O)* is attached to the surface via both nitrogen atoms [44], whereas the latter is hat-like attached to the surface via terminal nitrogen and oxygen atoms [45]. According to our recent DFT calculations [46], the former horse-like N_2O(a) can not dissociate directly to N_2(g)+O(a), but it rather transforms via highly tilted linear N-bonded TS into hat-like N_2O(a), which then dissociates into N_2 and O(a). Such a transformation of horse-like to hat-like N_2O via tilted N-bonded form is also compatible with the

DFT study of Ricart et al [47]. Thus, we may even expect in some specific cases different desorption dynamics of N_2 in the NO reduction from that in the N_2O reduction/decomposition, in particular, when nascent N_2O(a) in the former reaction displays different adsorption structures from that of the latter, because several stable forms with very similar adsorption energy have been recently predicted for adsorbed N_2O [46,48].

Cho (kinetically) and Belton (with IR spectroscopy) drew negligible re-adsorption of N_2O on NO- or CO-covered surfaces [13,39]. It is noteworthy that this intermediate N_2O is formed in the adsorption state. The branching as a result of the subsequent decomposition/desorption is largely due to the difference in the activation energy between both processes and co-adsorbed species; i.e., it does not involve an adsorption process of gaseous N_2O. Thus, the participation of this intermediate in the NO reduction cannot be examined from the reactivity of gaseous N_2O.

4.2 N_2 emission channel change

For the formation of intermediate N_2O(a), NO(a) must partly dissociate to yield N(a). The N_2 formation via N_2O(a) is noticeable at around 410 K, much below the temperature of 490 K estimated with high-resolution electron energy loss spectroscopy [30]. The overall reaction at low temperatures is controlled by either NO dissociation or N_2O(a) formation, since nitrogen-containing species (N(a) and NO(a) [30,36]) are present in a significant amount and both the decomposition and desorption of resultant N_2O(a) are so fast that it cannot be detected with surface spectroscopy [1,28,29]. On this surface, the dissociation of NO(a) and the reaction of NO(a)+N(a) proceed with comparable rates since a mixture of ^{15}N(a) and ^{14}NO(a) can be simply prepared just below the temperature of NO dissociation and desorption [6]. On the other hand, the recombination of N(a) is relatively enhanced at higher temperatures because of the high activation energy [1,5,49,50] and depleted NO(a) by increased desorption and dissociation [36]. Surface nitrogen atoms are also removed as ammonia, especially above the critical D_2 pressure.

The reaction of 2D(a)+O(a)$\rightarrow D_2O$(a) is very fast on Pd surfaces above 400 K [51]; i.e., either $\Theta_O >> \Theta_D$ or $\Theta_O << \Theta_D$ is possible in steady-state NO reduction under a high vacuum, where Θ_O and Θ_D stand for the coverage of O(a) and D(a), respectively. At lower temperatures or low D_2 pressures, the reaction of D(a) with O(a) is still very fast, providing unoccupied sites suitable for the adsorption and dissociation of NO as well as for the decomposition of N_2O(a). This enhances the NO dissociation with increasing D_2 pressure thus increasing the content of nitrogen atoms on the surface without accumulation of D(a) leading to the enhanced N_2O pathway. The amount of oxygen atoms deposited from NO(a) is significant below the critical point and is sharply suppressed above it because of the fast 2D(a)+O(a) reaction and depleted NO(a); i.e., at the transition point, the amounts of surface hydrogen and oxygen sharply change into the opposite directions. Thus, D(a) is accumulated above the kinetic transition point, and then the ammonia formation is enhanced and the

N_2O formation itself and its decomposition are reduced. The reaction with N(a) is not as fast as that with O(a), and the ammonia formation then competes with both N_2O formation and N-atom recombination, since its activation energy is in between the latter two processes.

In the N_2O pathway when CO is used, either N_2O formation or decomposition (NO dissociation as well) is retarded by CO(a) [1]. In fact, CO(a) remains significantly below about 500 K and occupies adsorption or dissociation sites. It removes O(a) as CO_2 but with a slower rate than hydrogen does [51,52], yielding slower switching of the amounts of CO(a) and O(a). Actually, no sharp critical point is found in the CO dependence for the NO+CO reaction.

A similar change of the N_2 emission channel is also observed on Pd(110) and Rh(100) in a slower manner [1,53]. The sharp change on Pd(211) is largely due to the enhanced N_2O pathway because both the reduced NO(a) and enhanced nitrogen removal as ammonia are also observed on Pd(110) where the N_2O pathway is not sharply enhanced [53]. The following factors may contribute to acceleration of this pathway; (i) Intermediate N_2O(a) dissociates rather than desorbs; i.e., it has higher selectivity to N_2 than that on Pd(110) [53]; and (ii) There is high accumulation of N(a) due to the rapid dissociation of NO(a) on stepped Pd(211) without hydrogen accumulation [30].

4.3 Off-normal N_2 emission

The mechanism of the inclined N_2 emission has not been fully understood, even in the dissociation of adsorbed N_2O on the widely studied Pd(110). The nascent product N_2 on Pd(211) may move in a way similar to that in the N_2O+CO (or H_2) reaction on Pd(110) and Rh(110) because of the similar spatial distribution [1,20,21,34].

The following findings are reported for the N_2O dissociation on Pd(110) [1,45]. (i) No N_2O is adsorbed through the terminal oxygen, and a tilting form through the terminal nitrogen is not reactive. (ii) Reactive N_2O is oriented along the [001] direction; this species is bent and bonded to the surface via terminal N and O atoms. (iii) The inclined N_2 desorption is initiated by the dissociation of N_2O, where the N-O bond is broken first.

Immediately after this bond rupture, the resultant nascent N_2 is attracted to the metal surface (the N_2-surface bond is similar in strength and length to the N_2O-surface bond) [45]. Nevertheless, the N-metal bond in the nascent product is likely to be broken before being thermalized/stabilized to the ground state because of considerable *repulsive forces* received from the counter product O(a). Indeed, off-normal N_2 emission is observed considerably below the desorption temperature of adsorbed N_2; i.e., at 85-100 K on Pd(110) [41,54], 100 K on Ir(110) [43], and about 60 K on Rh(110) [55]. Adsorbed N_2 is desorbed at around 120 K on Pd(110), 200 K on Ir(110) [43] and 160 K on Rh(110) [1]. Furthermore, consecutive N_2 emission after the N-O bond rupture is suggested from the spatial distribution highly concentrated around the normally directed plane along the orientation of the parent molecule. In the steady-state N_2O reduction on Pd(110) and Rh(110) as well as NO

reduction on Pd(110) below about 550 K, the N_2 distribution is sharp versus the azimuth angle shift, yielding a width of about 30° at half maximum [19-21]. This suggests the repulsive desorption from the site bonding to the nascent N_2 without transfers to other sites. After the N-O bond rupture, the nascent N_2 fragment is proposed to be swung over the bonding metal atom because of the repulsive force operative from the counter product oxygen. The sequential (delayed) break of the N-metal bond lets the N_2 fragment finally leave the surface. According to recent DFT-GGA calculations, the adsorption energy of N_2 to the metal surface is reduced with increasing the tilting of the molecular axis from the stable normal direction. The N_2-surface bond is the weakest at around 35° off normal on Pd(110) and Rh(110) [46], suggesting inclined desorption after the N_2 is swung over the bonding metal atom. The resultant collimation angle will be shifted more off normal over the weakest bonding angle when the repulsive forces from the counter oxygen are strong enough because of the presence of high kinetic energy (desorption before stabilization). Significant repulsive forces to the nascent N_2 have already been predicted on Pd(110) from DFT-GGA [45]. This will lead to larger collimation angles on surfaces with smaller work functions or smaller lattice constants because of the resultant more polarized or closer oxygen. Thus, by considering the extent of repulsive forces, we may explain the reported order of the collimation angles on different surfaces; i.e., 60-75° on Rh(110), 66-71° on Rh(100) [1] > 50-65° on Ir(110) [43,56] > 40-45° on Pd(110). The large angle shift is expected on Rh(110) and Rh(100) with a lower work function [57] and a smaller lattice constant, yielding the more polarized oxygen at closer distances than those on Pd(110). The shift on Ir(110) will be between the others because of the intermediate work function and lattice constant [57]. Generally, the collimation angle is affected from (i) the repulsive forces from the counter product O(a), (ii) the shape of the potential energy surface of the N_2(a) above the metal surface, and (iii) the amount of released energy and its partitioning [9]. The cumulative effect from these factors must be theoretically examined.

According to this model of the transition state for N_2O decomposition, we can examine active forms of N_2O(a) on the present surface because the off-normal (around -25°) N_2 emission has been reported in the N_2O decomposition on Pd(211) at around 110 K under AR-TPD conditions as well [34]. Its emission is highly concentrated in the plane along the step up-and-down direction. This collimation is close to that in the present work. A suitable candidate of adsorbed N_2O should be oriented along the $[\bar{1}11]$ direction; i.e., at the transition-state, the terminal oxygen atom will interact with step atoms so that the nascent N_2 is emitted over the (111) facet toward the (100) step normal side. According to preliminary DFT calculations, a suitable form of N_2O(a) is adsorbed through a terminal nitrogen atom and tilted in the $[\bar{1}11]$ direction toward the step edge. In the course of dissociation, the N_2O tilts further and bends with the terminal O toward the bridge site at the step edge, and the N-O bond concomitantly elongates [46]. The resulting transition state is similar to that

reported by Burch on Pt(211) [58]. The nascent N_2 emitted from the N_2O is swung in the $[1\bar{1}\bar{1}]$ direction toward the (111) facet and finally leaves the surface. The resultant collimation angle shifts toward the surface normal more than that on Pd(110) (40°-45° off normal) because of the inclination (19.5°) of the (111) facet and a similar distance between the product oxygen and the nascent N_2. Indeed the difference in the collimation angle between Pd(110) and Pd(211) is similar to the angle of inclination of the (111) facet of Pd(211).

5. Conclusions

The product N_2 distribution has been studied in the steady-state NO+D_2 reaction on stepped Pd(211) by angle-resolved desorption measurements. The following conclusions were reached.

(1) The desorbing N_2 is highly collimated at about 30° off normal toward the step down direction in the intermediate N_2O decomposition. On the other hand, it is broadly collimated near along the surface normal in the recombination of N(a).

(2) A sharp change of the N_2 emission channel from $N_2O(a)\rightarrow N_2(g)+O(a)$ to $N(a)+N(a)\rightarrow N_2(g)$ takes place at around 500 K. In the steady-state NO+CO reaction, the pathway gradually changes above 500 K. This channel change is promoted by hydrogen (deuterium) to limited extents.

(3) A model for the off-normal N_2 emission on late transition metals and an active intermediate N_2O form on Pd(211) have been proposed.

Acknowledgements

This work was partly supported by Grant-in-Aid No. 21550004 for General Scientific Research from the Japan Society for the Promotion of Science (JSPS). A. K. acknowledges the JSPS and *Slovenian Research Agency* for financing his research visit at AIST, Tsukuba in Japan.

.

R**eferences**

[1] T. Matsushima, Prog. Surf. Sci. 82 (2007) 435-477.

[2] M. Ikai, H. He, C.E. Borroni-Bird, H. Hirano, K.I. Tanaka, Surf. Sci. 315 (1994) L973-L976.

[3] M. Ikai, K.I. Tanaka, Surf. Sci. 357/358 (1996) 781-785.

[4] M. Ikai, N.M.H. Janssen, B.E. Nieuwenhuys, K.I. Tanaka, J. Chem. Phys. 106 (1997) 311-320.

[5] M. Ikai, K.I. Tanaka, J. Chem. Phys. 110 (1999) 7031-7036.

[6] M. Ikai, K.I. Tanaka, J. Phys. Chem. B, 103 (1999) 8277-8282.

[7] K.I. Tanaka, A. Sasahara, J. Mol. Catal. A, Chem. 155 (2000) 13-22.

[8] K.I. Tanaka, M. Ikai, Topics in Catal. 20 (2002) 25-33.

[9] T. Matsushima, K. Shobatake, J. Mol. Catal. A, Chem. 315 (2010) 135-147.

[10] C.T. Campbell, J.M. White, Appl. Surf. Sci. 1 (1978) 347-359.

[11] T.W. Root, L.D. Schmidt, G.B. Fisher, Surf. Sci. 134 (1983) 30-45.

[12] Se H. Oh, G.B. Fisher, J.E. Carpenter, D.W. Goodman, J. Catal. 100 (1986) 360-376.

[13] B.K. Cho, J. Catal. 148 (1994) 697-708.

[14] V.I. Pãrvulescu, P. Grange, B. Delmon, Catal. Today 46 (1998) 233-316.

[15] K. Watanabe, A. Kokalj, Y. Inokuchi, I. Rzeznicka, K. Ohshimo, N. Nishi, T. Matsushima, Chem. Phys. Lett. 406 (2005) 474-478.

[16] K. Watanabe, A. Kokalj, H. Horino, I.I. Rzeznicka, T. Takahashi, N. Nishi, T. Matsushima, Jpn. J. Appl. Phys. 45**,** Part 1(3B) (2006) 2290-2294.

[17] A. Kokalj, I. Kobal, T. Matsushima, J. Phys. Chem. B, 107 (2003) 2741-2747.

[18] A. Kokalj, T. Matsushima, J. Chem. Phys. 122 (2005) 34708(1-10).

[19] Y. Ma, T. Matsushima, K. Shobatake, A. Kokalj, J. Chem. Phys. 124 (2006) 144711(1-11).

[20] T. Kondo, M. Sakurai, T. Matsushima, J. Nakamura, J. Chem. Phys. 132 (2010) 134704 (1-9).

[21] M. Sakurai, T. Kondo, J. Nakamura, J. Chem. Phys. 134 (2011) 204710 (1-7).

[22] H. Wang, R.G. Tobin, C.L. DiMaggio, G.B. Fisher, D.K. Lambert, J. Chem. Phys. 107 (1997) 9569-9576.

[23] D.N. Belton, C.L. DiMaggio, S.J. Schmieg, K.Y. Simon Ng, J. Catal. 157 (1995) 559-568.

[24] A. Sasahara, H. Tamura, K.I. Tanaka, Catal. Lett. 28 (1994) 161-166.

[25] P. Granger, C. Dujardin, J.-F. Paul, G. Leclercq, J. Mol. Catal. A, Chem. 228 (2005) 241-253.

[26] O.M. Ilinitcha, L.V. Nosova, V.V. Gorodetskii, V.P. Ivanov, S.N. Trukhan, E.N. Gribov, S.V. Bogdanov, F.P. Cuperus, J. Mol. Catal. A, Chem. 158 (2000) 237-249.

[27] M. Hähnlein, U. Prüsse, S. Hörold, K.-D. Vorlop, Chemie Ingenieur Technik, 69 (1997) 90-93.

[28] E. Ozensoy, C. Hess, D.W. Goodman, J. Am. Chem. Soc. 124 (2002) 8524-8525.

[29] E. Ozensoy, D.W. Goodman, Phys. Chem. Chem. Phys. 6 (2004) 3765-3778.

[30] R.D. Ramsier, Q. Gao, H. Neergaard Waltenburg, K.-W. Lee, O.W. Nooij, L. Lefferts, J. T. Yates, Jr., Surf. Sci. 320 (1994) 209-237.

[31] P.W. Davies, R.M. Lambert, Surf. Sci. 110 (1981) 227-249.

[32] H.-D. Schmick, H.-W. Wassmuth, Surf. Sci. 123 (1982) 471-490.

[33] T. Matsushima, Surf. Sci. Rep. 52 (2003) 1-62.

[34] M. Sakurai, T. Matsushima, T. Kondo, J. Nakamura, Proc. of 106-th Catal. Soc. Jpn. Meeting A, 2010, 4H14 (in Japanese).

[35] A. Obuchi, S. Naito, T. Onishi, K. Tamaru, Surf. Sci. 122 (1982) 235-255.

[36] R.D. Ramsier, Q. Gao, H. Neergaard Waltenburg, J. T. Yates, Jr., J. Chem. Phys. 100 (1994) 6837-6845.

[37] V.P. Zhdanov, B. Kasemo, Surf. Sci. Rep. 29 (1997) 31-90.

[38] C.H.F. Pedan, D.N. Belton, S.J. Schmieg, J. Catal. 155 (1995) 204-218.

[39] H. Permana, K.Y. Simon Ng, C.H.F. Peden, S.J. Schmieg, D.K. Lambert, D.N. Belton, J. Catal. 164 (1996) 194-206.

[40] A.V. Zeigarnik, Kinet. Catal. 44 (2003) 233-246.

[41] H. Horino, S. Liu, A. Hiratsuka, Y. Ohno, T. Matsushima, Chem. Phys. Lett. 341 (2001) 419-424.

[42] C. Kodama, H. Orita, H. Nozoye, Appl. Surf. Sci. 121/122 (1997) 579-582.

[43] H. Horino, I.I. Rzeznicka, A. Kokalj, I. Kobal, Y. Ohno, A. Hiratsuka, T. Matsushima, J. Vac. Sci. Technol. A 20 (2002) 1592-1596.

[44] R. Burch, S.T. Daniels, P. Hu, J. Chem. Phys. 117 (2002) 2902-2908.

[45] I. Kobal, A. Kokalj, H. Horino, Y. Ohno, T. Matsushima, Trends in Chem. Phys. 10 (2002) 139-178.

[46] A. Kokalj, H. Orita, in preparation.

[47] J.M. Ricart, F. Ample, A. Clotet, D. Curulla, J.W. (Hans) Niemantsverdriet, J.F. Paul, J. Pérez-Ramírez, J. Catal. 232 (2005) 179-185.

[48] H. Orita, T. Kubo, T. Matsushima, A. Kokalj, J. Phys. Chem. C, 114 (2010) 21444-21449.

[49] M.J.P. Hopstaken, J.W. Niemantsverdriet, J. Phys. Chem. B, 104 (2000) 3058-3066.

[50] D.N. Belton, C.L. DiMaggio, K.Y. Simon Ng, J. Catal. 144 (1993) 273-284.

[51] T. Engel, H. Kuipers, Surf. Sci. 90 (1979) 181-196.

[52] T. Engel, G. Ertl, J. Chem. Phys. 69(1978) 1267-1281.

[53] Y.-S. Ma, T. Matsushima, J. Phys. Chem. B, 109 (2005) 1256-1261.

[54] S. Haq, A. Hodgson, Surf. Sci. 463 (2000) 1-10.

[55] K. Imamura, T. Matsushima, Catal. Lett. 97 (2004) 197-202.

[56] Our recent AR-work shows that in a steady state N_2O+CO reaction on Ir(110), the desorption of the product N_2 is split into two components in the plane along the [001] direction as a form of $\cos^{10}(\cos(\theta-\theta_0)+\cos^{10}(\theta+\theta_0)$ at 500 K-700 K with θ_0=50º-60º.

[57] H.B. Michaelson, J. Appl. Phys. 48 (1977) 4729-4733.

[58] R. Burch, S.T. Daniells, J.P. Breen, P. Hu, J. Catal. 224 (2004) 252-260.

Figure Captions

Fig. 1 Top and side views of stepped Pd(211), definition of crystal axes, and the definition of the desorption angle, θ.

Fig. 2 Surface temperature dependence of AI product signals and AR $^{15}N_2$ signals at -31° off normal in a steady-state $^{15}NO+D_2$ reaction with P_{NO}= 1.5×10^{-5} Pa and P_{D2}= (a) 1.2×10^{-5} Pa and (b) 3.2×10^{-4} Pa. The temperature was increased stepwise to 800 K and then decreased. AR-N_2 signals observed in the direction of increasing surface temperature are designated by filled squares and those in the downward direction by open squares. Only AI signals in the direction of increasing temperature are shown for clarity. No D_2O signals are shown in (b) because of the large uncertainty in the presence of a high D_2O background. AI-N_2: ▲, D_2O:○, N_2O:◇, ND_3:▽, and AR-$^{15}N_2$: ■, □.

Fig. 3 (a) Traces of the AR-N_2 signal at -31° off normal in the heating and subsequent cooling in the presence of a $^{15}NO+D_2$ mixture (P_{NO}= 1.5×10^{-5} Pa, and (i) P_{D2}= 4.4×10^{-5} Pa or (ii) 1.1×10^{-5} Pa). Angular distributions of desorbing $^{15}N_2$ in the plane along the step up-and-down direction; (b) peak at 490 K and (c) desorption at 600 K. Typical deconvolutions are shown by broken curves. The solid lines indicate the summation. The value of *R* represents the ratio between the maximum signals of the resultant broad and sharp components.

Fig. 4 Angular distributions of desorbing $^{15}N_2$ in the plane along the step up-and-down direction in the $^{15}NO+D_2$ reaction at T_S=450-590 K. The steady-state ^{15}NO + D_2 reaction was established at P_{NO}= 1.5×10^{-5} Pa and P_{D2}= 2.9×10^{-5} Pa. The surface temperature is (a) 450 K, (b) 478 K, (c) 500 K and (d) 590 K. The signals observed in the direction of the increasing desorption angle (from the negative region toward the positive) are designated by closed symbols, and those in the decreasing desorption angle, by open symbols. Typical deconvolutions are shown by broken curves. The solid lines indicate the summation. The value of *R* represents the ratio between the maximum signals of the resultant broad and sharp components.

Fig. 5 Variation of the product AI mass signals and the AR-$^{15}N_2$ signals at -31° off normal in the steady-state NO reduction with D_2 pressures. The vertical lines indicate the kinetic transition point. The signals observed in the direction of the increasing D_2 pressure are designated by closed symbols, and those in the decreasing pressure, by open symbols. AI-N_2:▲,△, D_2O:●,○, N_2O:◆,◇, ND_3:▼, ▽, and AR-$^{15}N_2$: ■,□.

Fig. 6 (a) T_S dependence of AI product signals and AR $^{15}N_2$ signal at -30° off normal in a steady-state $^{15}NO+^{13}CO$ reaction with $P_{NO}=1.5\times10^{-5}$ Pa and $P_{CO}=2.9\times10^{-5}$ Pa. Signals observed in the direction of the increasing surface temperature are designated by filled symbols, and those in the downward direction, by open symbols. Angular distributions of desorbing products in the plane along the step up-and-down direction; (b) $^{13}CO_2$ at 530 K, (c) $^{15}N_2$ at 531 K, and (d) $^{15}N_2$ at 475 K. The signals observed in the direction of the increasing desorption angle are designated by closed symbols, and those in the decreasing desorption angle, by open symbols. Typical deconvolutions are shown by broken curves. The solid lines indicate the summation. The value of *R* represents the ratio of the maximum signals of the resultant components.

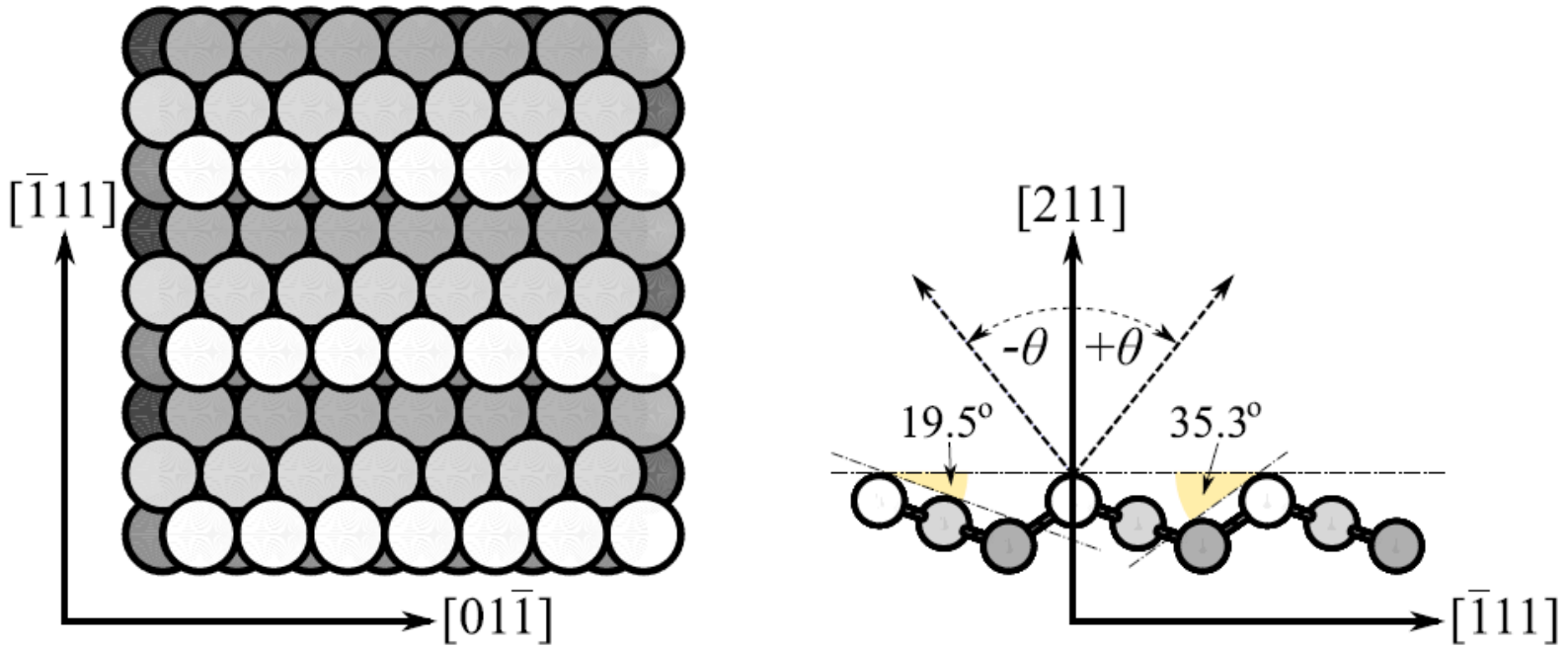

Fig.1 Mat

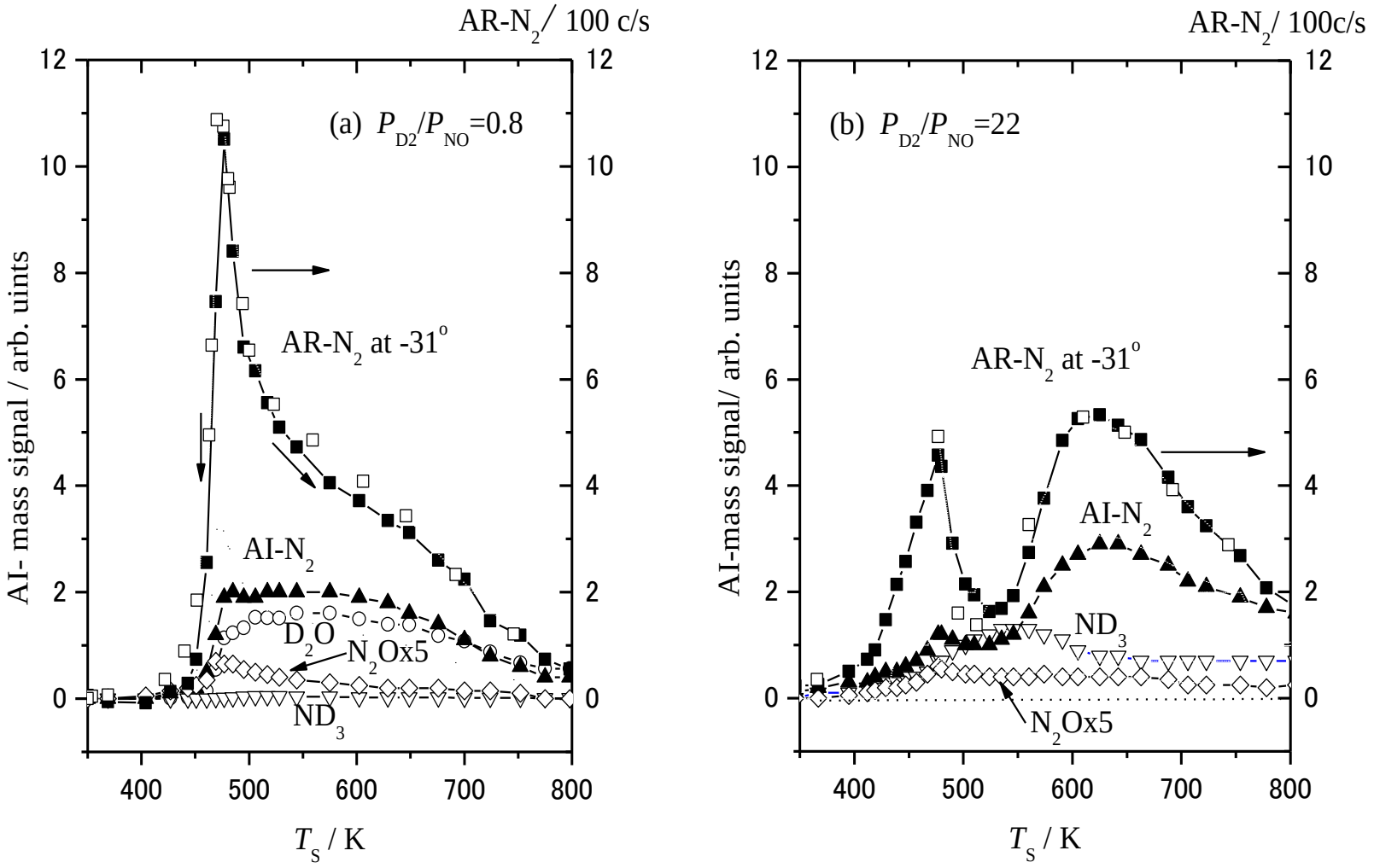
AR-N2/ 100 c/s
(a) PD2/PNO=0.8
AR-N2 at -31°
AI-N2
D2O
N2Ox5
ND3
AI- mass signal / arb. uints
TS / K
AR-N2/ 100c/s
(b) PD2/PNO=22
AR-N2 at -31°
AI-N2
ND3
N2Ox5
AI-mass signal/ arb. units
TS / K

Fig. 2 Mat

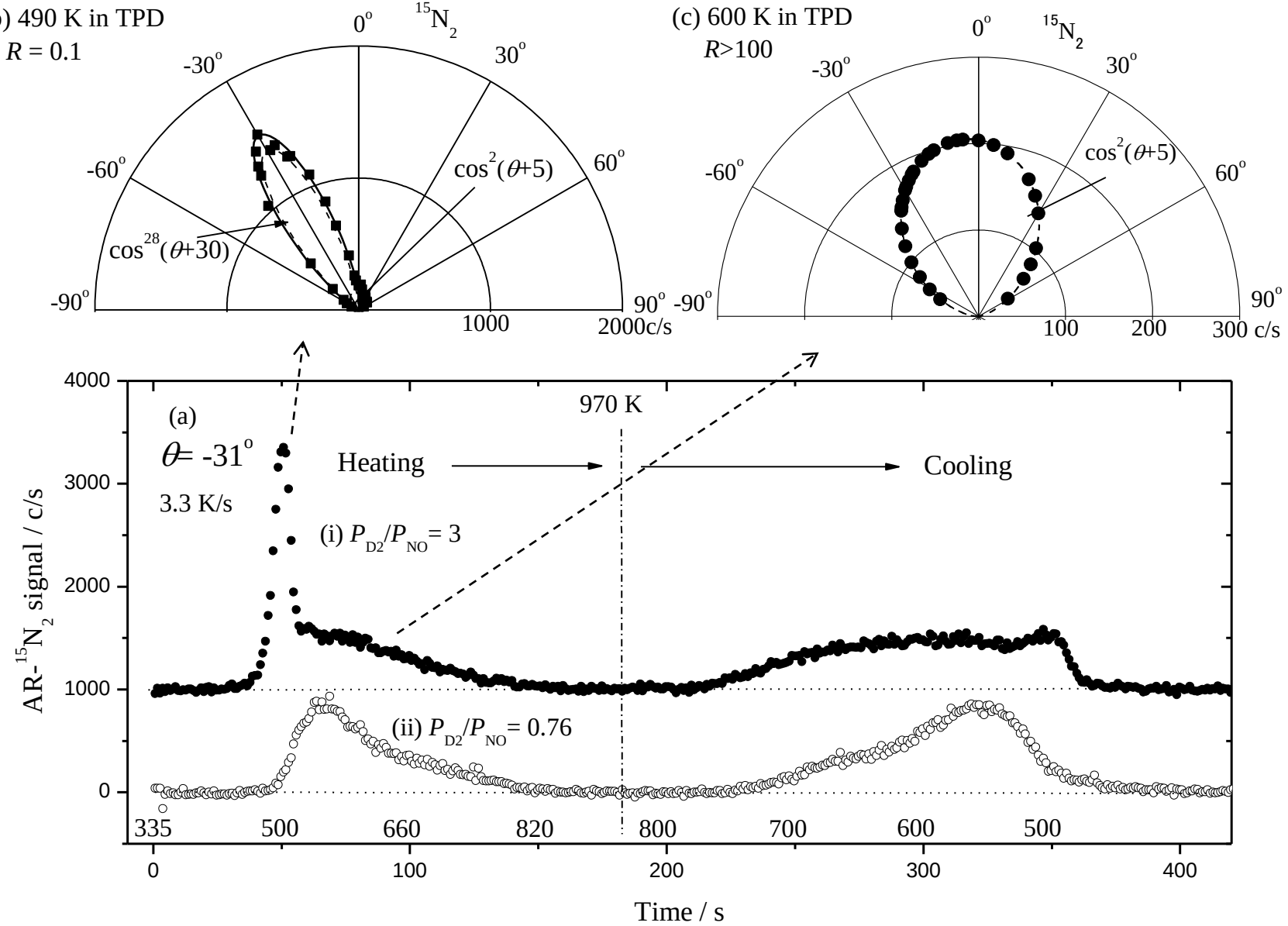
(b) 490 K in TPD
R = 0.1
15N2
0°
30°
-30°
60°
-60°
90°
-90°
cos2(θ+5)
cos28(θ+30)
1000
2000c/s
(c) 600 K in TPD
R>100
15N2
100
200
300 c/s
(a)
θ= -31°
3.3 K/s
970 K
Heating
Cooling
(i) PD2/PNO= 3
(ii) PD2/PNO= 0.76
AR-15N2 signal / c/s
Time / s
335
500
660
820
800
700
600
500

Fig. 3 Mat

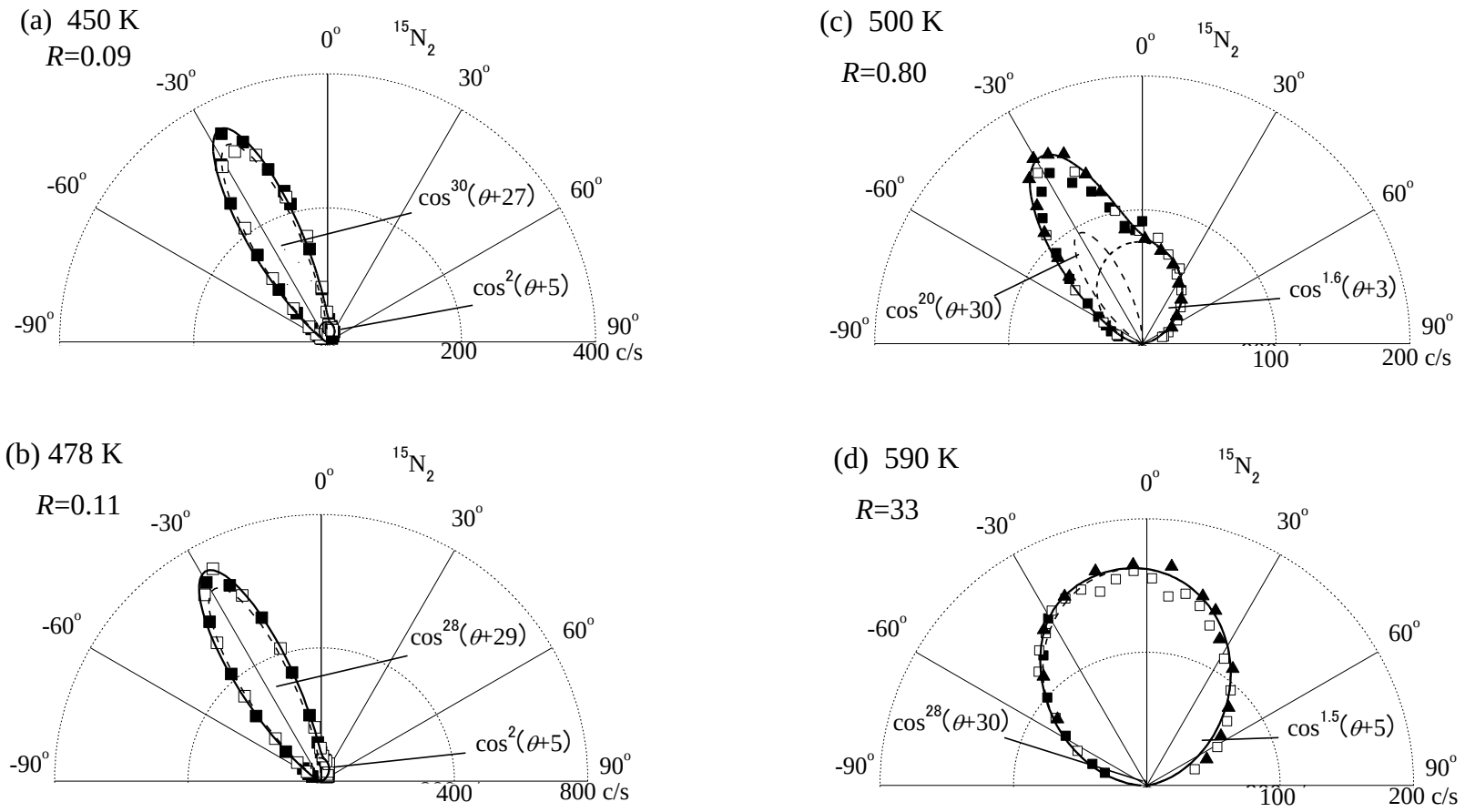
(a) 450 K
R=0.09
0°
15N2
-30°
30°
-60°
60°
cos30(θ+27)
cos2(θ+5)
-90°
90°
200
400 c/s
(c) 500 K
R=0.80
0°
15N2
-30°
30°
-60°
60°
cos20(θ+30)
cos1.6(θ+3)
-90°
90°
100
200 c/s
(b) 478 K
R=0.11
0°
15N2
-30°
30°
-60°
60°
cos28(θ+29)
cos2(θ+5)
-90°
90°
400
800 c/s
(d) 590 K
R=33
0°
15N2
-30°
30°
-60°
60°
cos28(θ+30)
cos1.5(θ+5)
-90°
90°
100
200 c/s

Fig. 4 Mat

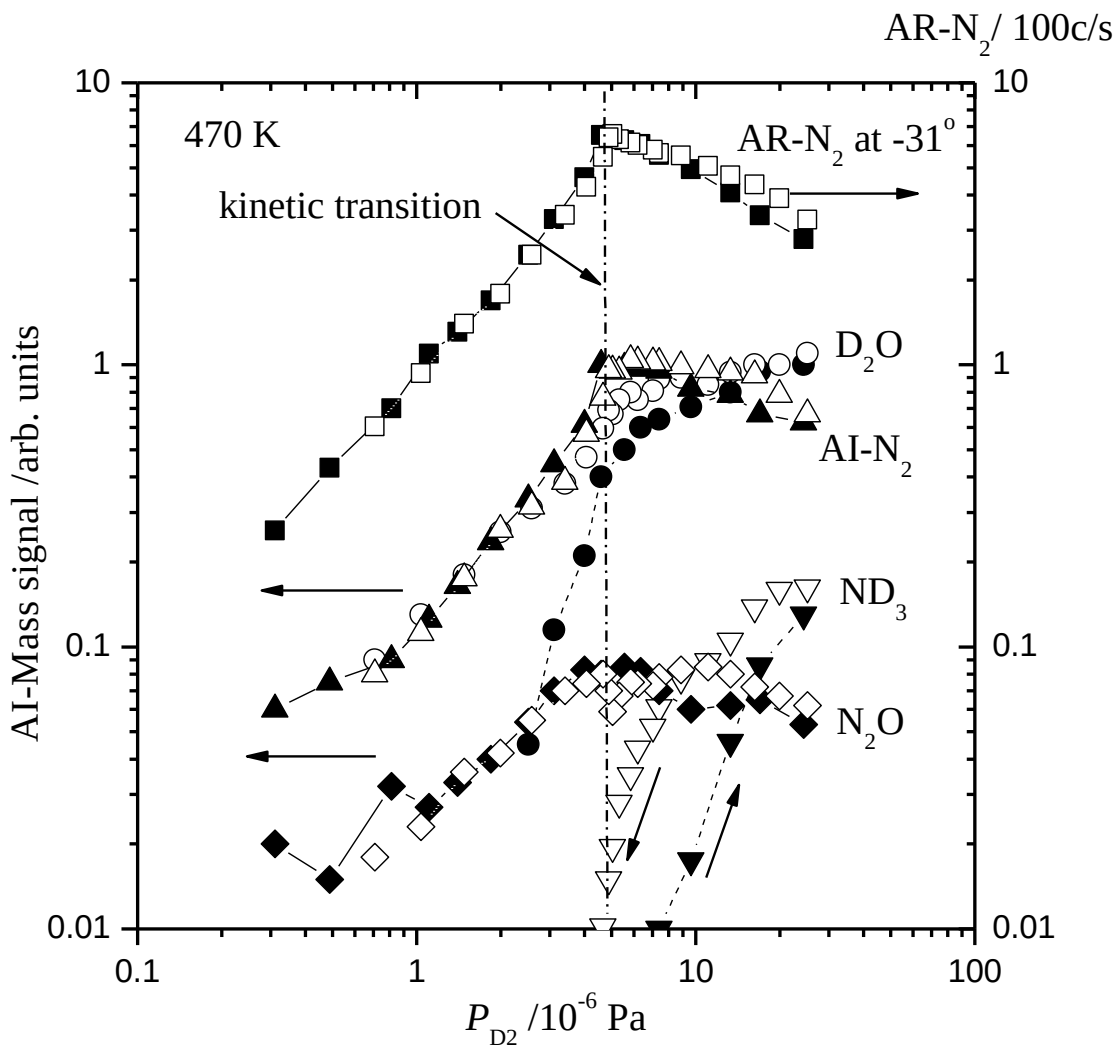
AR-N2/ 100c/s
470 K
AR-N2 at -31°
kinetic transition
D2O
AI-N2
ND3
N2O
AI-Mass signal /arb. units
P D2 /10-6 Pa
10
1
0.1
0.01
0.1
1
10
100

Fig. 5 Mat

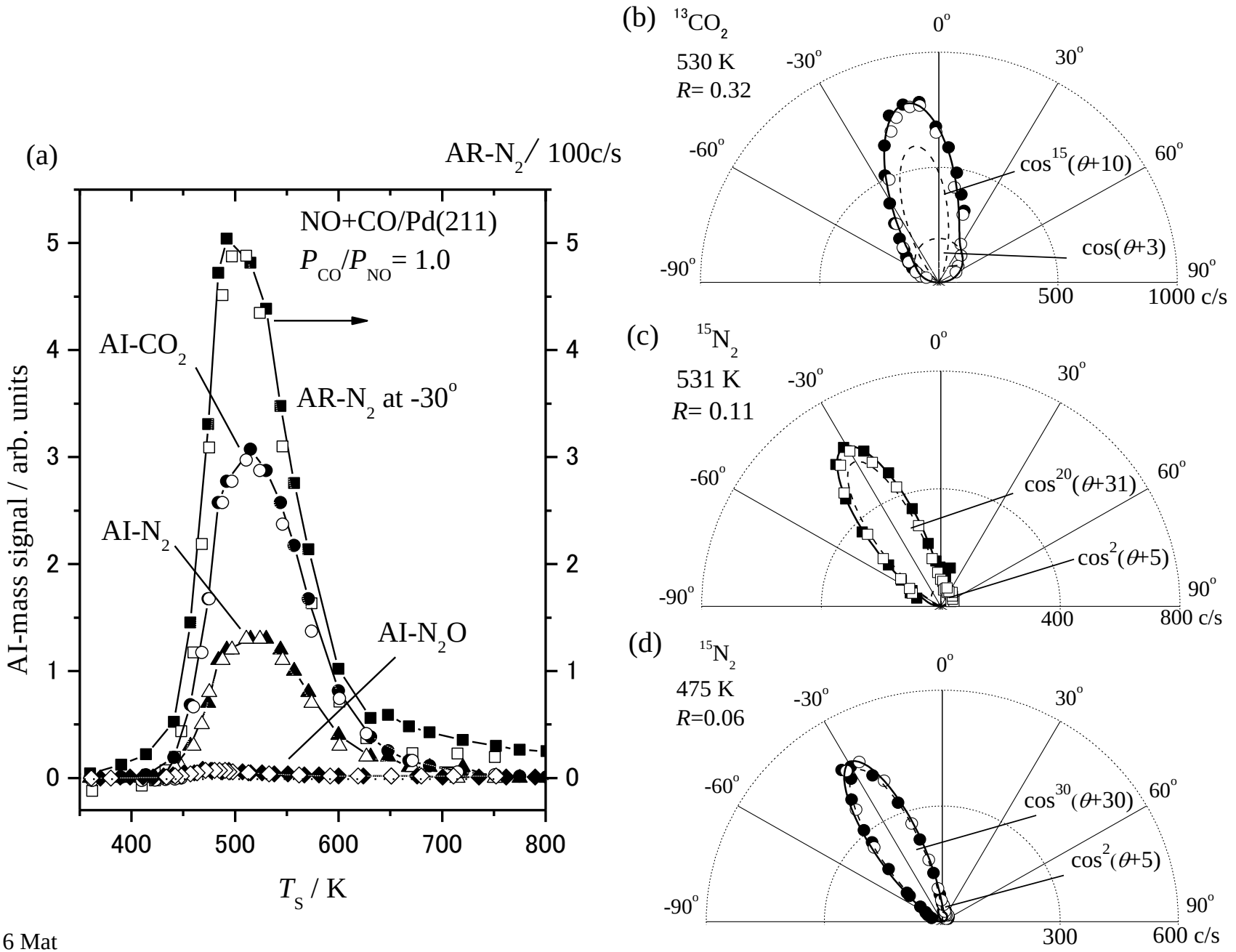
(a)
AR-N2/ 100c/s
NO+CO/Pd(211)
PCO/PNO= 1.0
AI-CO2
AR-N2 at -30°
AI-N2
AI-N2O
AI-mass signal / arb. units
TS / K
(b) 13CO2
530 K
R= 0.32
cos15(θ+10)
cos(θ+3)
500
1000 c/s
(c) 15N2
531 K
R= 0.11
cos20(θ+31)
cos2(θ+5)
400
800 c/s
(d) 15N2
475 K
R=0.06
cos30(θ+30)
cos2(θ+5)
300
600 c/s

Fig. 6 Mat